

Spectrally-resolved quantum interferometry for absolute and high-precision determination of optical properties

Florian Kaiser^{1,*}, Panagiotis Vergyris¹, Djeylan Aktas¹,

Charles Babin^{1,2}, Laurent Labonté¹, and Sébastien Tanzilli¹

¹*Université Côte d'Azur, CNRS, Laboratoire de Physique de la Matière Condensée, France*

²*École Normale Supérieure de Lyon, 46 Allée d'Italie, 69364 Lyon Cedex 07, France*

Quantum optical metrology exploits superpositions of N -photon number states, referred to as $N00N$ -states, for phase sensing with N times improved sensitivity compared to classical approaches involving N photons. Here, we introduce the concept of spectrally-resolved quantum white-light interferometry based on energy-time entangled two-photon $N00N$ -states as a tool for optical property measurements. We apply this method to measure chromatic dispersion in an optical fibre and demonstrate that employing such quantum states of light leads not only to better precision, but also to absolute parameter determination. Notably, by comparing the quantum method to state-of-the-art classical realizations, we show a 2.6 times better precision, despite involving 60 times less photons on average. This underlines that the improved results are essentially due to conceptual advantages enabled by quantum optics which are likely to define new standards in a variety of applied research fields.

INTRODUCTION

Optical phase-sensing

Optical phase-sensing stands as one of the most advanced techniques in classical metrology and has recently led to the direct detection of gravitational waves [1]. From the applied side, phase-sensitive spectrally-resolved white-light interferometry (WLI) is a key enabling tool for improving optical technologies finding numerous applications in physics, medicine, and biology. In the perspectives of both research and development, WLI has been exploited for high-precision measurements such as distance and displacement [2], strain, temperature and pressure [3], surface profilometry [4], refractometry [5], group delay dispersion [6], as well as chromatic dispersion [7–13].

The optimal precision for measuring an unknown phase ϕ in an optical interferometer using classical light is ruled by the standard quantum limit, $\delta\phi \sim 1/\sqrt{N}$, where N is the average number of photons involved in the measurement. The precision can be further improved by using quantum light, *e.g.* so-called $N00N$ -states which represent a coherent supersposition of having N photons in one optical mode with zero in an orthogonal mode, and vice versa. This permits reaching the Heisenberg limit, $\delta\phi \sim 1/N$ [14–21]. However, due to experimental imperfections, such as optical losses, noise and non-unity detector efficiencies, most of today's real-world measurements operate far away from these fundamental limits.

We introduce and demonstrate here spectrally-resolved quantum white-light interferometry (Q-WLI) as a novel approach for absolute and high-precision measurements of optical properties. The peculiar use of energy-time entangled two-photon $N00N$ -states permits achieving significant conceptual advantages compared to standard WLI, allowing absolute determination of optical param-

eters. Additionally, both data treatment and experimental procedures are greatly simplified, making this method ready to be exploited as an enabling tool in a large variety of fields.

Standard white-light interferometry

As shown in FIG. 1(a), the emission of a white-light source is usually directed to an interferometer in which the reference arm is free-space (with well known optical properties) and the other arm comprises the sample under test (SUT). Recombining both arms at the output beam-splitter leads to an interference pattern for which the intensity follows $I \propto 1 + \cos(\phi(\lambda))$, with $\phi(\lambda) = \frac{2\pi}{\lambda} (L_r - n(\lambda) \cdot L_s)$. Here, λ represents the wavelength, L_r and L_s are the physical lengths of the reference arm and the SUT, respectively, and $n(\lambda)$ is the refractive index of the SUT. It is worth noting that interference is only observed when the interferometer is balanced within the coherence length of the white-light source, or the coherence length imposed by the resolution of the spectrometer, which is typically on the order of microns to millimetres [22, 23]. In this case, the phase term reads (more details are given in the supplementary information):

$$\phi(\lambda_0 + \Delta\lambda) \approx 2\pi L_s \left(\frac{1}{2} \frac{d^2 n}{d\lambda^2} \cdot \frac{(\Delta\lambda)^2}{\lambda_0 + \Delta\lambda} + \frac{1}{6} \frac{d^3 n}{d\lambda^3} \cdot \frac{(\Delta\lambda)^3}{\lambda_0 + \Delta\lambda} \right) + \phi_{\text{off}}. \quad (1)$$

Here, λ_0 stands for the symmetry center of the fringe pattern, usually referred to as stationary phase point [22, 23], $\Delta\lambda$ is the wavelength offset compared to λ_0 , and ϕ_{off} is a constant offset phase. Fitting experimentally acquired data as a function of $\Delta\lambda$ allows inferring L_s , and/or the

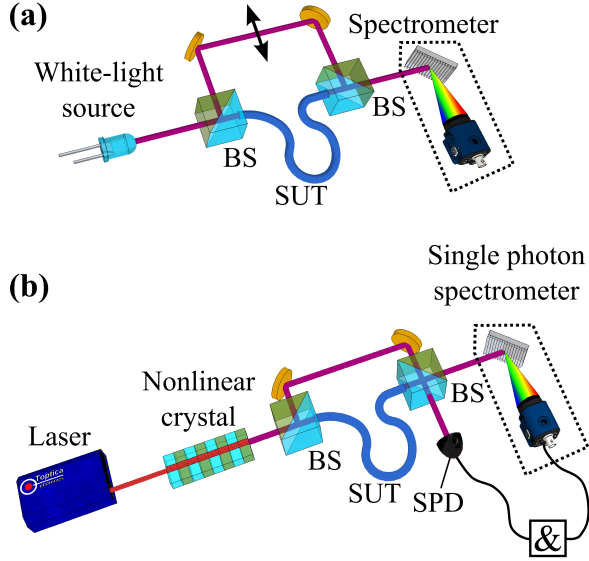


FIG. 1. Typical experimental setups for standard spectrally-resolved WLI (a), and Q-WLI (b). BS, beam-splitter; SUT, sample under test; SPD, single photon detector. &-symbol, time-tagging and coincidence logic.

optical material parameters $\frac{d^2n}{d\lambda^2}$ and $\frac{d^3n}{d\lambda^3}$. Assuming that L_s is precisely known, a typical fit to the data requires three free parameters, *i.e.* λ_0 , $\frac{d^2n}{d\lambda^2}$ and $\frac{d^3n}{d\lambda^3}$, which are usually all interdependent in a non-trivial fashion. Consequently, uncertainties on one parameter induce errors on the others. In fact, the high number of required fitting parameters and the necessity to re-equilibrate the interferometer for every new SUT stand as the main issues of this technique, therefore limiting its precision and potential for absolute determination of optical properties, as well as its ease-of-use [12, 24].

However, more accurate optical measurements are eagerly demanded in almost all fields where optics is involved. A special focus is set on the material parameter $\frac{d^2n}{d\lambda^2}$, as it is directly related to the chromatic dispersion coefficient $D = -\frac{\lambda_0}{c} \cdot \frac{d^2n}{d\lambda^2}$, in which c represents the speed of light [6–13]. More accurate measurements on D would have tremendous repercussions for optimizing today's telecommunication networks, developing new-generation pulsed lasers and amplifiers, designing novel linear and nonlinear optical components and circuits, as well as for assessing the properties of biological tissues.

MATERIALS AND METHODS

Quantum white-light interferometry

FIG. 1(b) shows the experimental schematic for our new concept of spectrally-resolved quantum WLI (Q-WLI), intended to overcome the above-mentioned is-

ssues. The quantum white-light source is composed of a continuous-wave pump laser and a non-linear crystal in which energy-time entangled photon pairs are generated through spontaneous parametric downconversion [25]. This process obeys the conservation of the energy, *i.e.* $\frac{1}{\lambda_p} = \frac{1}{\lambda_1} + \frac{1}{\lambda_2}$. Here, λ_p represents the wavelength of the pump laser photons, and $\lambda_{1,2}$ are the wavelengths of the individual photons for each generated pair. Another implication of the conservation of the energy is that the degenerate wavelength of the emission spectrum is $\lambda_0 = 2\lambda_p$.

The paired photons are sent to the interferometer which is, intentionally, strongly unbalanced. This allows distinguishing contributions for which both photons take opposite paths (delayed arrival times at the interferometer's outputs) or the same path (no arrival time difference) [26]. At one interferometer output, a single photon detector (SPD) is employed, and in the other a single-photon sensitive spectrometer. Time tagging electronics allows to infer the photon arrival time differences, and to post-select only zero-time-delay events. This procedure leads to the formation of a two-photon *NOON*-state:

$$|\psi\rangle = \frac{(|2\rangle_r|0\rangle_s + e^{i\phi_{N00N}}|0\rangle_r|2\rangle_s)}{\sqrt{2}}. \quad (2)$$

Here, the ket vectors, indexed by *s* and *r*, indicate the number of photons in the reference and SUT arm, respectively, and $\phi_{N00N} = \phi(\lambda_1) + \phi(\lambda_2)$. As detailed in the supplementary information, after setting $\lambda_2 = \lambda_0 + \Delta\lambda$, the spectral dependence of the phase term ϕ_{N00N} is given by:

$$\phi_{N00N}(\lambda_0 + \Delta\lambda) \approx \frac{d^2n}{d\lambda^2} \cdot \frac{\pi L_s \cdot (\Delta\lambda)^2}{\frac{\lambda_0}{2} + \Delta\lambda} + \phi_{\text{off}}, \quad (3)$$

in which $\phi_{\text{off}} = \frac{4\pi(n(\lambda_0)L_s - L_r)}{\lambda_0}$ is an offset term. In order to infer ϕ_{N00N} , a two-photon coincidence measurement is performed, taking advantage of the fact that the rate R at which pairs are projected onto the *N00N*-state is phase-dependent: $R \propto 1 + \cos(\phi_{N00N})$. The term ϕ_{off} has been object of research in the past [27–29], as it allows measuring optical phase-shifts at constant wavelengths with doubled sensitivity compared to the standard approach. By taking advantage of energy-time entanglement, we address here, for the first time, the wavelength-dependent term in equation 3. Experimentally, this is made possible by recording R as a function of $\Delta\lambda$, *i.e.* the two-photon coincidence rate is measured as a function of the paired-photons' wavelengths.

We now highlight a few pertinent purely quantum-enabled features provided by equation 3. Compared to equation 1, the dependence on the third-order term $\frac{d^3n}{d\lambda^3}$ is cancelled due to energy-time entanglement [30]. Furthermore, λ_0 does not have to be extracted from the data, as it is exactly twice the wavelength of the continuous-wave pump laser, λ_p , and can therefore be known with

extremely high accuracy. This means that the quantum strategy allows data fitting using exactly one free parameter, namely $\frac{d^2n}{d\lambda^2}$ which is an essential step towards absolute optical property determination with high precision. Additionally, we note that the $N00N$ -state's ability to interfere does not arise from the coherence length of the individual photons, but from that of the photon pair. For energy-time entanglement, this coherence length is directly related to that of the continuous wave pump laser (typically from several to hundreds of meters) [25]. This allows to operate the interferometer in largely unbalanced conditions, such that no re-alignment is necessary when changing the SUT. Finally, due to the use of a two-photon $N00N$ -state, a doubled sensitivity on $\frac{d^2n}{d\lambda^2}$ is achieved, allowing to perform measurements on much shorter samples compared to standard WLI (down to the mm to cm scale).

Detailed optical setup and data acquisition

As a SUT we use a 1 m long standard single-mode fibre from Corning (SMF28e). For all measurements, the interferometer is actively stabilized using a reference laser and a piezoelectric transducer on one of the mirrors in the reference arm (more details are provided in the methods section). This ensures that ϕ_{off} remains constant. For chromatic dispersion measurements using standard WLI, a superluminescent diode is used. At the output of the interferometer we measure an average spectral intensity of ~ 125 pW/nm from 1450–1650 nm. Interferograms are recorded using a standard spectrometer from Anritsu (model MS9710B) with 0.1 s integration time and 0.5 nm resolution.

For the Q-WLI approach, the employed light source is made of a wavelength-stabilized 780.24 nm laser, pumping a type-0 periodically-poled lithium niobate waveguide (PPLN/W). The quasi-phase matching in the PPLN/W is chosen such as to generate energy-time entangled photon pairs around the degenerate wavelength of $\lambda_0 = 1560.48$ nm with a bandwidth of about 140 nm. Here, the spectral intensity is about 25 fW/nm at the interferometer output. To detect the paired photons, we use an InGaAs SPD (IDQ 220) at one interferometer output. The single photon spectrometer at the other output is made of a wavelength-tunable 0.5 nm bandpass filter, followed by another InGaAs SPD (IDQ 230). To partially compensate for the significantly reduced spectral intensity of the photon pair source, we use an integration time of 8 s.

All measurements are repeated 100 times on the same SUT in order to infer the statistical accuracy of both WLI and Q-WLI approaches.

RESULTS AND DISCUSSION

Statistical analysis for comparing measurement accuracy

Typical interference patterns for chromatic dispersion measurements using both methods are shown in FIG. 2(a,b). With the Q-WLI setup, twice as much interference fringes are obtained for the same spectral bandwidth which is a direct consequence of the doubled phase sensitivity of the two-photon $N00N$ -state. After

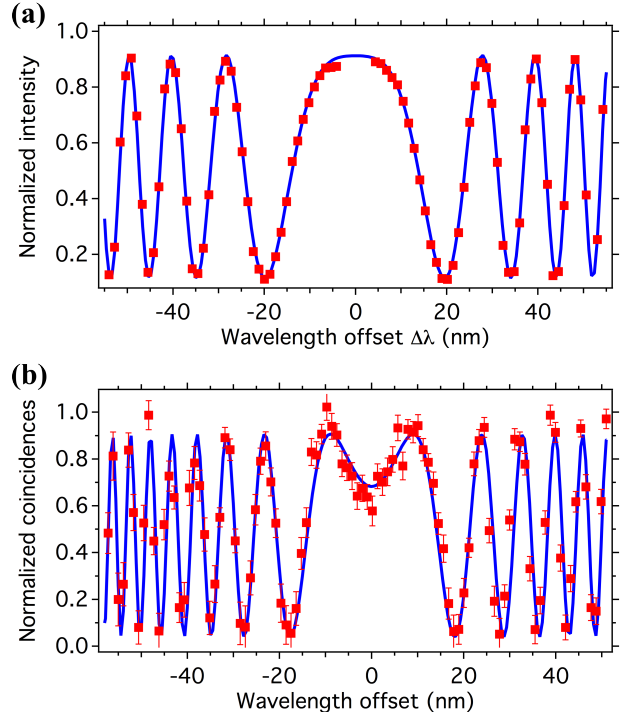


FIG. 2. Typical measurements when inferring chromatic dispersion in a 1 m long standard single-mode fibre using standard WLI (a), and Q-WLI (b). Red dots, data points; Blue lines, appropriate fits to the data from which D is extracted. Error bars assume poissonian photon number statistics.

acquiring 2×100 measurements on the same SUT, we infer the precision of both approaches. The results of the statistical data analysis are shown in FIG. 3. For standard WLI, we obtain, on average, $D = 17.047 \frac{\text{ps}}{\text{nm} \cdot \text{km}}$ at $\lambda_0 \approx 1560.5$ nm with a standard deviation of $\sigma_{\text{classical}} = 0.051 \frac{\text{ps}}{\text{nm} \cdot \text{km}}$. This result is amongst the best reported to date in the literature [7–13]. For Q-WLI, we measure, on average, $D = 17.035 \frac{\text{ps}}{\text{nm} \cdot \text{km}}$ at $\lambda_0 = 1560.48$ nm with a significantly better standard deviation of $\sigma_{N00N} = 0.021 \frac{\text{ps}}{\text{nm} \cdot \text{km}}$. Further statistical data analysis shows Kurtosis parameters of 0.182 and 0.276 for standard and quantum WLI, respectively, proving that both data sets converge towards a normal distribution. Comparing the data sets with Levene's null hypothesis test gives $p < 5 \cdot 10^{-4}$,

providing very strong evidence that the improved results obtained with the quantum strategy are essentially impossible to have occurred based on random sampling from the classical measurements.

In our data, we observe a minimal offset of the central values which is explained by either a slight wavelength offset of the spectrometer (< 0.2 nm) used for the standard measurements, and/or that the interferometer was unbalanced by about $1.5 \mu\text{m}$. The consequence is an error on the fitting parameter λ_0 , which is then translated to an error in $\frac{d^2n}{d\lambda^2}$ [22, 23]. At this point, we highlight that for the Q-WLI approach, λ_0 is essentially known with absolute accuracy, and only one free fitting parameter is required. Additionally, an unbalanced interferometer does not influence the measurement. It is therefore natural to consider that Q-WLI can be used to determine the chromatic dispersion coefficient with absolute accuracy.

We also emphasize that the measurements performed with Q-WLI involve ~ 60 times less photons transmitted through the SUT compared to standard WLI. This clearly underlines that the improved results obtained with the entanglement-enhanced strategy is due to aspects from both the fundamental and conceptual sides.

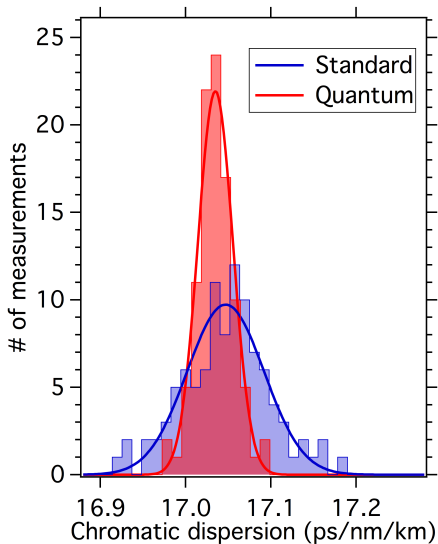


FIG. 3. Histogram of inferred chromatic dispersion coefficients after 100 repetitions on the same SUT using both standard (blue) and entanglement-enhanced (red) measurements, respectively. Fits to the data assume a normal distribution.

Device calibration using Q-WLI

Another advantage provided by Q-WLI lies in straightforward device calibration. All the optical components in the interferometer actually show small residual chromatic dispersion, and this undesired offset needs to be

evaluated and subtracted from the data in order to avoid systematic errors. For standard WLI, this implies that the SUT has to be removed and that the length of the reference arm has to be reduced accordingly (typically on the order of 1 m). This procedure is technically challenging, time-consuming, and might lead to additional systematic errors.

At this point, Q-WLI shows its ability for user-friendly operation. Interference is observed for interferometer path length differences up to the coherence length of the pump laser, in our case ~ 250 m. Consequently, residual chromatic dispersion can be measured directly after removing the SUT, without any realignment. FIG. 4

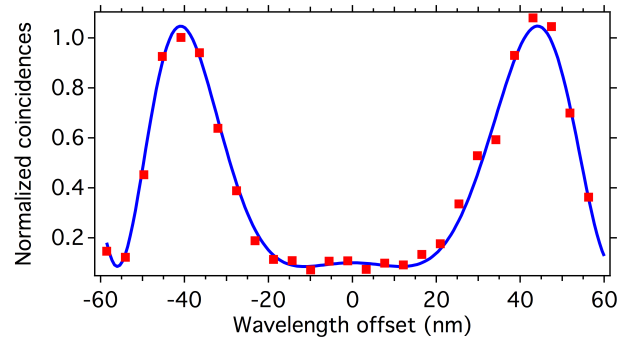


FIG. 4. Experimental results when using Q-WLI for inferring residual chromatic dispersion in our interferometer without the SUT. Red dots, data points; Blue lines, appropriate fit to the data.

shows the experimental results that we have obtained when measuring chromatic dispersion in our bare interferometer, *i.e.* with the SUT. It turns out that in our interferometer, residual chromatic dispersion amounts to $\sim 10\%$ of the measured values on the 1 m SUT. For all the data discussed above, except for the raw data in FIG. 2(a,b), we have therefore subtracted the residual chromatic dispersion.

CONCLUSIONS

We have introduced and demonstrated the concept of spectrally-resolved Q-WLI exploiting energy-time entangled two-photon $N00N$ -states. Compared to standard measurements, the $N00N$ -state permits achieving a two times higher phase sensitivity. More strikingly, the peculiar use of such quantum states of light reduces the number of free parameters for fitting experimental data from three to one, representing a major advantage for determining optical properties with high precision and absolute accuracy. In addition, our setup does not require a balanced interferometer for performing the measurement which represents a significant time-saving advantage compared to standard WLI, especially for device calibration and when considering measurements on

a large set of samples.

As an exemplary demonstration, we have applied our scheme to infer chromatic dispersion in a standard single-mode fibre, obtaining 2.6 times more precise results compared to state-of-the-art realizations, despite using ~ 60 times less photons.

We note that the sensitivity of our approach could be further doubled by using a double-pass configuration [8], towards measurements on short samples, such as optical components and waveguide structures (mm to cm length scale). Such measurements would also be of interest for medical applications where precise knowledge on chromatic dispersion in tissues is required to yield optimal image quality in optical coherence tomography [31]. In this perspective, the reduced number of photons required for quantum white-light interferometry is also highly interesting for measurements performed on photosensitive biological samples [32–34]. Regarding optical telecommunication systems, by rotating the polarization of the entangled photon pairs, our setup could be also used for measuring polarization mode dispersion in optical components, which would lead to refinement of manufacturing processes. In the end, ultimate measurement accuracy at the Heisenberg limit would be reached by deterministically generating $N00N$ -states [35], combined with near-unity efficiency superconducting single photon detectors [36].

We therefore believe that combining fundamental and conceptual advantages enabled by quantum light is a very promising approach for the future development and improvement of applications requiring absolute and high-accuracy measurements of optical properties.

* florian.kaiser@unice.fr

- [1] LIGO Scientific Collaboration and Virgo Collaboration, “Observation of gravitational waves from a binary black hole merger,” *Phys. Rev. Lett.*, vol. 116, p. 061102, 2016.
- [2] U. Schnell, E. Zimmermann, and R. Dandliker, “Absolute distance measurement with synchronously sampled white-light channelled spectrum interferometry,” *Pure Appl Opt: Europ Opt Soc P A*, vol. 4, p. 643, 1995.
- [3] K. Totsu, Y. Haga, and M. Esashi, “Ultra-miniature fiber-optic pressure sensor using white light interferometry,” *J. Micromech. Microeng.*, vol. 15, p. 71, 2005.
- [4] J. Calatroni, A. Guerrero, C. SÁñinz, and R. Escalona, “Spectrally-resolved white-light interferometry as a profilometry tool,” *Opt Laser Technol*, vol. 28, pp. 485 – 489, 1996.
- [5] C. Sainz, J. E. Calatroni, and G. Tribillon, “Refractometry of liquid samples with spectrally resolved white light interferometry,” *Meas. Sci. Technol.*, vol. 1, p. 356, 1990.
- [6] A. P. Kovács, R. Szipöcs, K. Osvay, and Z. Bor, “Group-delay measurement on laser mirrors by spectrally resolved white-light interferometry,” *Opt. Lett.*, vol. 20, pp. 788–790, 1995.
- [7] P. Hlubina, M. Szpulak, D. Ciprian, T. Martynkien, and W. Urbanczyk, “Measurement of the group dispersion of the fundamental mode of holey fiber by white-light spectral interferometry,” *Opt. Express*, vol. 15, pp. 11073–11081, 2007.
- [8] L. Labonté, P. Roy, D. Pagnoux, F. Louradour, C. Restoin, G. Mélin, and E. Burov, “Experimental and numerical analysis of the chromatic dispersion dependence upon the actual profile of small core microstructured fibres,” *J Opt A-Pure Appl Opt*, vol. 8, pp. 933–938, 2006.
- [9] T. M. Kardaś and C. Radzewicz, “Broadband near-infrared fibers dispersion measurement using white-light spectral interferometry,” *Opt. Commun*, vol. 282, pp. 4361–4365, 2009.
- [10] P. Hlubina, M. Kadulová, and P. Mergo, “Chromatic dispersion measurement of holey fibres using a supercontinuum source and a dispersion balanced interferometer,” *Opt Laser Eng*, vol. 51, pp. 421–425, 2013.
- [11] Q. Ye, C. Xu, X. Liu, W. H. Knox, M. F. Yan, R. S. Windeler, and B. Eggleton, “Dispersion measurement of tapered air-silica microstructure fiber by white-light interferometry,” *Appl. Opt.*, vol. 41, pp. 4467–4470, 2002.
- [12] T. Grosz, A. P. Kovacs, M. Kiss, and R. Szipocs, “Measurement of higher order chromatic dispersion in a photonic bandgap fiber: comparative study of spectral interferometric methods,” *Appl. Opt.*, vol. 53, pp. 1929–1937, 2014.
- [13] M. A. Galle, W. S. Mohammed, L. Qian, and P. W. Smith, “Single-arm three-wave interferometer for measuring dispersion of short lengths of fiber,” *Opt. Express*, vol. 15, pp. 16896–16908, 2007.
- [14] V. Giovannetti, S. Lloyd, and L. Maccone, “Quantum-enhanced measurements: beating the standard quantum limit,” *Science*, vol. 306, pp. 1330–1336, 2004.
- [15] P. Walther, J.-W. Pan, M. Aspelmeyer, R. Ursin, S. Gasparoni, and A. Zeilinger, “De Broglie wavelength of a non-local four-photon state,” *Nature*, vol. 429, pp. 158–161, 2004.
- [16] M. W. Mitchell, J. S. Lundeen, and A. M. Steinberg, “Super-resolving phase measurements with a multiphoton entangled state,” *Nature*, vol. 429, pp. 161–164, 2004.
- [17] T. Nagata, R. Okamoto, J. L. O’Brien, K. Sasaki, and S. Takeuchi, “Beating the standard quantum limit with four-entangled photons,” *Science*, vol. 316, pp. 726–729, 2007.
- [18] B. L. Higgins, D. W. Berry, S. D. Bartlett, H. M. Wiseman, and G. J. Pryde, “Entanglement-free Heisenberg-limited phase estimation,” *Nature*, vol. 450, pp. 393–396, 2007.
- [19] J. C. F. Matthews, A. Politi, A. Stefanov, and J. L. O’Brien, “Manipulation of multiphoton entanglement in waveguide quantum circuits,” *Nat Photon*, vol. 3, pp. 346–350, 2009.
- [20] I. Afek, O. Ambar, and Y. Silberberg, “High-NOON states by mixing quantum and classical light,” *Science*, vol. 328, pp. 879–881, 2010.
- [21] V. Giovannetti, S. Lloyd, and L. Maccone, “Advances in quantum metrology,” *Nature Photon.*, vol. 5, pp. 222–229, 2011. and references therein.
- [22] K. Naganuma, K. Mogi, and H. Yamada, “Group-delay measurement using the Fourier transform of an interferometric cross correlation generated by white light,” *Opt. Lett.*, vol. 15, pp. 393–395, 1990.
- [23] S. Diddams and J.-C. Diels, “Dispersion measurements

- with white-light interferometry,” *J. Opt. Soc. Am. B*, vol. 13, pp. 1120–1129, 1996.
- [24] M. A. Galle, *Virtual Reference Interferometry: Theory & Experiment*. PhD thesis, Department of Electrical & Computer Engineering, University of Toronto, 2014.
 - [25] J. D. Franson, “Bell inequality for position and time,” *Phys. Rev. Lett.*, vol. 62, pp. 2205–2208, 1989.
 - [26] F. Kaiser, A. Issautier, L. A. Ngah, O. Alibart, A. Martin, and S. Tanzilli, “A versatile source of polarization entangled photons for quantum network applications,” *Laser Phys Lett*, vol. 10, pp. 045202(1–7), 2013.
 - [27] A. Crespi, M. Lobino, J. C. F. Matthews, A. Politi, C. R. Neal, R. Ramponi, R. Osellame, and J. L. O’Brien, “Measuring protein concentration with entangled photons,” *Appl. Phys. Lett.*, vol. 100, p. 233704, 2012.
 - [28] T. Ono, R. Okamoto, and S. Takeuchi, “An entanglement-enhanced microscope,” *Nat. Commun.*, vol. 4, p. 2426, 2013.
 - [29] Y. Israel, S. Rosen, and Y. Silberberg, “Supersensitive polarization microscopy using NOON states of light,” *Phys. Rev. Lett.*, vol. 112, p. 103604, 2014.
 - [30] M. B. Nasr, B. E. A. Saleh, A. V. Sergienko, and M. C. Teich, “Dispersion-cancelled and dispersion-sensitive quantum optical coherence tomography,” *Opt. Express*, vol. 12, pp. 1353–1362, 2004.
 - [31] W. Drexler, U. Morgner, F. X. Kärtner, C. Pitris, S. A. Boppart, X. D. Li, E. P. Ippen, and J. G. Fujimoto, “In vivo ultrahigh-resolution optical coherence tomography,” *Opt. Lett.*, no. 17, pp. 1221–1223, 1999.
 - [32] M. M. Frigault, J. Lacoste, J. L. Swift, and C. M. Brown, “Live-cell microscopy – tips and tools,” *Journal of Cell Science*, vol. 122, pp. 753–767, 2009.
 - [33] M. Celebrano, P. Kukura, A. Renn, and V. Sandoghdar, “Single-molecule imaging by optical absorption,” *Nat. Photon.*, vol. 5, pp. 95–98, 2011.
 - [34] M. Piliarik and V. Sandoghdar, “Direct optical sensing of single unlabelled proteins and super-resolution imaging of their binding sites,” *Nat. Commun.*, vol. 5, p. 4495, 2014.
 - [35] I. Herbauts, B. Blauensteiner, A. Poppe, T. Jennewein, and H. Hübel, “Demonstration of active routing of entanglement in a multi-user network,” *Opt. Express*, vol. 21, pp. 29013–29024, 2013.
 - [36] R. H. Hadfield, “Single-photon detectors for optical quantum information applications,” *Nat Photon*, vol. 3, pp. 696–705, 2009. and references therein.
 - [37] F. Kaiser, L. A. Ngah, A. Issautier, T. Delord, D. Aktas, V. D’Auria, M. P. D. Micheli, A. Kastberg, L. Labonté, O. Alibart, A. Martin, and S. Tanzilli, “Polarization entangled photon-pair source based on quantum nonlinear photonics and interferometry,” *Opt. Commun.*, vol. 327, pp. 7–16, 2014. Special Issue on Nonlinear Quantum Photonics.
 - [38] J. Y. Lee and D. Y. Kim, “Versatile chromatic dispersion measurement of a single mode fiber using spectral white light interferometry,” *Opt. Express*, vol. 14, pp. 11608–11615, 2006.

ACKNOWLEDGEMENTS

The authors acknowledge financial support from the Foundation Simone & Cino Del Duca, the Euro-

pean Commission for the FP7-ITN PICQUE project (grant agreement No 608062), l’Agence Nationale de la Recherche (ANR) for the CONNEQT, SPOCQ and SITQOM projects (grants ANR-EMMA-002-01, ANR-14-CE32-0019, and ANR-15-CE24-0005, respectively), and the iXCore Research Foundation. We also thank M. T. Pérez Zaballos for help on statistical data treatment, as well as T. Debuisschert and A. Levenson for fruitful discussions.

AUTHOR CONTRIBUTIONS

F.K. established the theoretical framework and initiated the research. F.K., C.B. and L.L. set up the experiment. F.K., D.A. and P.V. performed data acquisition and treatment. F.K. and S.T. supervised the project. F.K. and S.T. drafted the manuscript. All authors contributed in finalizing the manuscript.

ADDITIONAL INFORMATION

Competing financial interests: The authors declare no competing financial interests.

METHODS

Mach-Zehnder interferometer stabilization

Without active interferometer phase stabilization, we observe 2π phase drifts every few seconds due to temperature drifts in the laboratory. This limits severely the integration times for both the classical and quantum measurements. Therefore, we employ an active phase stabilization system. It is made of an actively wavelength-stabilized 1560.5 nm reference laser sent in the counter-propagating way through the interferometer, and a piezoelectric translation stage in the reference arm of the interferometer [37]. The feedback loop has a bandwidth of 100 Hz which results in a long-term phase stability of $< \frac{2\pi}{40}$ rad.

Spatial and polarization mode overlap

In order to obtain high-visibility interference patterns at the interferometer output, the photon (or photon pair) contributions from both interferometer arms need to be made indistinguishable in both the spatial and polarization modes. Spatial mode overlap is ensured by using a fibre-optic beam-splitter at the interferometer output and input [38]. Polarization mode overlap is obtained using fibre-optic polarization controllers in both interferometer arms. These components are not shown in the main text figures in order to simplify the reading of the manuscript.

Quality of the entangled photon pair source

We infer the entanglement quality of our photon pair source in the following configuration. We fix the analysis wavelength of the spectrometer at 1550 nm and post-select the desired $N00N$ -state by a coincidence measurement. Then, the path length difference of the MZI is scanned and the two-photon coincidence rate is recorded. We measure sinusoidal oscillations with a raw fringe visibility of $87.1 \pm 2.2\%$ which increases to $95.5 \pm 2.6\%$ after the subtraction of detectors' dark counts. In other words, we obtain a fidelity of 97.8% to the desired $N00N$ -state. We explain imperfections by unbalanced losses between the two arms of the interferometer and multi-pair contributions.

Normalization of intensity and coincidence spectrograms

For the classical strategy, normalization is obtained by recording two reference spectrograms with either interferometer arm being blocked. Normalization is obtained

by dividing the data by the sum of both reference spectrograms.

For the entanglement-enabled strategy, we normalize the coincidence counts by taking advantage of the *undesired* contributions in which the paired photons take opposite paths inside the interferometer. These contributions do not interfere at the interferometer output, such that the related (non-zero time delay) coincidence rate is directly proportional to the spectral intensity of the photon pair generator. Normalization is obtained by dividing the $N00N$ -state coincidences by two times the sum of the non- $N00N$ -state coincidences.

Home-made single-photon spectrometer

As a single-photon spectrometer, we use a wavelength tunable motorized bandpass filter (Yenista XTM-50) followed by a low noise single-photon avalanche photodiode (id quantique id230) operated at 25% detection efficiency. The transmission loss of the filter is measured to be 4 dB such that the total quantum efficiency of the single-photon spectrometer is $\sim 10\%$.

SUPPLEMENTARY INFORMATION

Derivation of the fitting function for standard WLI

As outlined in the manuscript, the wavelength dependent phase shift at the interferometer output is

$$\phi(\lambda) = \frac{2\pi}{\lambda} (L_r - n(\lambda) \cdot L_s). \quad (4)$$

We approximate now $n(\lambda)$ by a third order Taylor series: $n(\lambda) = n(\lambda_0 + \Delta\lambda) \approx n(\lambda_0) + \sum_{k=1}^3 \frac{1}{k!} \frac{d^k n}{d\lambda^k} \cdot (\Delta\lambda)^k$. This leads to

$$\begin{aligned} \phi(\lambda_0 + \Delta\lambda) \approx 2\pi L_s & \left(\frac{n(\lambda_0)}{\lambda_0 + \Delta\lambda} + \frac{dn}{d\lambda} \cdot \frac{\Delta\lambda}{\lambda_0 + \Delta\lambda} \right. \\ & + \frac{1}{2} \frac{d^2 n}{d\lambda^2} \cdot \frac{(\Delta\lambda)^2}{\lambda_0 + \Delta\lambda} + \frac{1}{6} \frac{d^3 n}{d\lambda^3} \cdot \frac{(\Delta\lambda)^3}{\lambda_0 + \Delta\lambda} \Bigg) \\ & - \frac{2\pi L_r}{\lambda_0 + \Delta\lambda}. \end{aligned} \quad (5)$$

Note that, in general, the interference fringes obtained at the interferometer output are usually too closely spaced to be resolved by a commercial spectrometer because of the strong phase-dependence on zero and first order derivatives. In order to cancel these terms, the interferometer has to be precisely equilibrated to the so-called stationary phase point (SPP), which is found at $L_r = (n(\lambda_0) - \frac{dn}{d\lambda} \cdot \lambda_0) L_s$. Note that this point has to be found individually for each new sample with an accuracy on the order of a few micron. After finding the SPP, the dominant term is $\frac{d^2 n}{d\lambda^2}$ and the phase term simplifies to

$$\begin{aligned} \phi(\lambda_0 + \Delta\lambda) \approx 2\pi L_s & \left(\frac{1}{2} \frac{d^2 n}{d\lambda^2} \cdot \frac{(\Delta\lambda)^2}{\lambda_0 + \Delta\lambda} \right. \\ & \left. + \frac{1}{6} \frac{d^3 n}{d\lambda^3} \cdot \frac{(\Delta\lambda)^3}{\lambda_0 + \Delta\lambda} \right) + \phi_{\text{off}}, \end{aligned} \quad (6)$$

in which $\phi_{\text{off}} = 2\pi L_s \frac{dn}{d\lambda}$ is a constant phase offset. Assuming that L_s is known precisely, the required fitting parameters are therefore $\frac{d^2 n}{d\lambda^2}$, $\frac{d^3 n}{d\lambda^3}$ and λ_0 .

Data fitting up to $\frac{d^2 n}{d\lambda^2}$ and $\frac{d^3 n}{d\lambda^3}$

Data obtained with standard WLI require a fitting function taking into account terms up to $\frac{d^3 n}{d\lambda^3}$ to obtain the most precise and accurate results.

Fitting the data with the function described in equation 6 leads to $D = 17.047 \frac{\text{ps}}{\text{nm} \cdot \text{km}}$ at $\lambda_0 \approx 1560.5 \text{ nm}$ and $\sigma_{\text{classical}} = 0.051 \frac{\text{ps}}{\text{nm} \cdot \text{km}}$ after 100 measurements on the same standard single-mode fibre.

A fitting function taking into account only terms up to $\frac{d^2 n}{d\lambda^2}$ is does not lead to a good overlap between data

and experiment (see FIG. 5) which leads to both an off-set and a larger standard deviation, *i.e.* $D = 17.070 \pm 0.054 \frac{\text{ps}}{\text{nm} \cdot \text{km}}$.

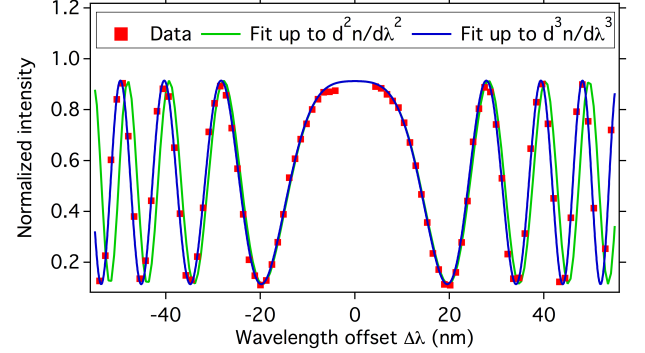


FIG. 5. Fitting standard WLI data (red dots) with a function taking into account terms up to $\frac{d^2 n}{d\lambda^2}$ (green line) and $\frac{d^3 n}{d\lambda^3}$ (blue line). Only the later shows a perfect overlap with the experimental data.

Derivation of the fitting function for Q-WLI

For the Q-WLI, the phase term is given by the two-photon phase $\phi_{N00N} = \phi(\lambda_1) + \phi(\lambda_2)$, which can be calculated using equation 4. Respecting the conservation of the energy, *i.e.* $\frac{1}{\lambda_p} = \frac{2}{\lambda_0} = \frac{1}{\lambda_1} + \frac{1}{\lambda_2}$, and setting $\lambda_2 = \lambda_0 + \Delta\lambda$ leads to

$$\begin{aligned} \phi_{N00N}(\lambda_0 + \Delta\lambda) \approx 2\pi L_s & \cdot \left(\frac{1}{2} \frac{d^2 n}{d\lambda^2} \cdot \frac{(\Delta\lambda)^2}{\frac{\lambda_0}{2} + \Delta\lambda} \right. \\ & \left. + \frac{1}{6} \frac{d^3 n}{d\lambda^3} \cdot \frac{(\Delta\lambda)^4}{\left(\frac{\lambda_0}{2} + \Delta\lambda\right)^2} \right) + \phi_{\text{off}}, \end{aligned} \quad (7)$$

where we consider the phase offset $\phi_{\text{off}} = \frac{4\pi(n(\lambda_0)L_s - L_r)}{\lambda_0}$ to be constant thanks to the active phase stabilization system. Let us stress the four important features in equation 7 compared to equation 6.

First, zero and first order derivatives are automatically cancelled, and therefore no SPP has to be found.

Second, for $\Delta\lambda \ll \lambda_0$, a twofold enhanced sensitivity on the second order dispersion term is obtained, which is a typical signature of $N00N$ -states.

Third, the third order dispersion term is strongly suppressed by a factor of about $\frac{2\Delta\lambda}{\lambda_0}$, which means that it can be generally neglected, except for really exotic samples with extraordinarily high third order dispersion.

Fourth, $\lambda_0 = 2\lambda_p$ is essentially known with arbitrary accuracy such that it has not to be considered as a fitting parameter.

Therefore, Q-WLI requires only one free parameter to fit the data, *i.e.* $\frac{d^2 n}{d\lambda^2}$.